Optimization of deformable mirror actuator geometry using machine learning methods

Oleg Soloviev[a,b]

[a]DCSC, ME, TU Delft, Mekelweg 2, 2624 CD Delft, the Netherlands
[b]Flexible Optical BV, Polakweg 10–11, 2288 GG Rijswijk, the Netherlands

ABSTRACT

The ability of a membrane deformable mirror to accurately reproduce a predefined range of aberrations is strongly affected by the geometry of its actuator layout. In this presentation, we consider ways to formalize the problem of finding the optimal actuator geometry and show how algorithms from image processing and machine learning can be applied. We illustrate the approach through a case study of a 79-channel membrane deformable mirror developed for the 14AMI project.

Keywords: Deformable mirror; actuator layout optimisation; residual aberration minimisation; Mumford-Shah functional; k-means clustering

1. INTRODUCTION

Adaptive Optics (AO) aims to correct for an optical aberration in the system with an AO element.[1] The quality of the correction is defined by the match of the statistics of the expected aberrations and the response space of the adaptive element,[2,3] the wavefront sensing error,[4] and there are a lot of publications in the literature devoted to these problems. However, most publications consider the problem of the correction quality from the user point of view: for instance, estimating the residual aberration for a particular AO hardware or from a theoretical point of view assuming an ideal AO correction with a given number of degrees of freedom.[5,6]

In this work, we consider the problem from the point of view of the AO manufacturer. The technology used to fabricate a deformable mirror primarily defines the characteristics of the response function space. For example, membrane mirrors have been shown to be more suitable for ophthalmic applications, while piezoelectric mirrors are better for atmospheric turbulence.[7] Besides the number of actuators and the aperture size, the technology can provide another freedom in the mirror design. For instance, for micromachined membrane deformable mirrors (MMDM),[8] where actuators are just area electrodes on a printed circuit board, it is relatively easy to change the layout geometry of these electrodes, with the only limitations given by the final distance (minimal gap) between the electrodes and the maximal mirror aperture. It is thus possible to adjust the actuator layout for a given application, especially if the statistics of the expected aberration are known. However, the problem is not presented well in the literature, and often, some heuristic approach is used, such as a uniform actuator layout in a regular hexagonal grid or a concentric structure with an equal number of actuators per ring (as in Fig. 1a).

This work presents a more systematic approach developed by Flexible Optical BV in an attempt to meet the demanding requirements on aberration correction quality in the framework of the EC-funded 14AMI project.[9] In this project, a membrane deformable mirror will be used in a wavefront sensor-less setup inside a quality check tool for the semiconductor industry to correct residual aberration and increase the imaging contrast.

The rest of the paper is organized as follows.

First, we describe the method of estimating the maximal correction error, that is, the remaining aberration resulting from approximation by a membrane mirror with a given actuator geometry of an arbitrary aberration sampled from a given distribution. In addition, we consider the influence of a non-zero mirror bias (required for the uni-directional membrane mirrors) and show that the maximal error can be estimated using the SVD method.

Further author information:
E-mail: oleg@okotech.com

Adaptive Optics and Wavefront Control for Biological Systems XI, edited by
Thomas G. Bifano, Na Ji, Lei Tian, Proc. of SPIE Vol. 13328, 1332802
 · 0277-786X · doi: 10.1117/12.3042094

Secondly, we consider the space spanned by the responses of the membrane deformable mirror depending on the given actuator geometry and discuss the consequences of the technology limitations, such as the finite gap between the actuators. The space can be calculated for each geometry, but solving the Poisson equation separately for each actuator can be time-consuming.

Then, we formalize the problem of finding the best actuator layout geometry as an optimization problem. To our knowledge, no methods exist in the literature for solving the original optimization problem. As the straightforward black-box optimization methods are not applicable due to the computation time, we propose to solve a relaxed version obtained by taking the Laplacian of the original problem. The relaxed problem is shown to be related to the simplified Mumford-Shah functional[10,11] and does not require the costly calculation of the mirror responses. We demonstrate, compare, and discuss the results obtained with the existing image processing and machine learning methods based on the minimum variance and the data clustering.

Finally, we consider another relaxation of the problem by imposing concentrically constraints on the actuator geometry and applying clustering methods to define the optimal radii of the actuator geometry.

In conclusion, we present the experimental results demonstrating the response functions obtained from a fabricated mirror prototype. The technique of mirror characterization is described in the other presentation of this conference (Paper No. BO506-27[12]).

2. PROBLEM FORMULATION

The requirements on the correction quality of the mirror were provided to us in the form of a table, specifying the aberration to be corrected in terms of its maximum expected *rms* amplitude z_i, $i = 1, \ldots, 25$ of its decomposition in the first 25 Zernike polynomials, and the maximal correction error. Loosely formulated, our task is to design a deformable mirror that can approximate or correct for any input aberration from this range with an approximation error not greater than some ϵ_{max}. The other requirements of the partners (mirror reflectivity, aperture diameter, and the feed-forward type of the control) defined the possible mirror fabrication technology to be a micromachined membrane deformable mirror (MMDM) due to its zero hysteresis feature. The maximum number of actuators to be used was not specified.

With these parameters specified, we needed to obtain an actuator layout that would correct the input aberration within the given error.

To formalize this problem, we made a standard assumption on the linearity of the mirror correction, that is, that all possible mirror shapes are located in the subspace spanned by the mirror response functions. Thus, to determine the maximum error, we need to find the maximum distance between the set of possible input aberrations and its best approximation by the mirror responses. We begin by describing the mirror responses for the chosen technology.

2.1 Space of the MMDM responses

The shape w of the membrane deformable mirror is approximated by the solution of the Poisson equation with the Dirichlet conditions

$$\Delta\ w(x,y) = c\ V^2(x,y), \quad w\ |_{\partial\Omega} = 0, \tag{1}$$

where V describes the voltage distribution on the actuators, c is some constant defined by the physical parameters of the mirror, and Ω is the membrane area.[13]

For an MMDM, the voltage is constant on the area of each actuator, so the curvature of the mirror shape is 1) piece-wise constant, 2) is equal to zero in the regions where no actuator is present, and 3) is always non-negative. The last condition implies that all the shapes should be considered with respect to some middle surface, called *bias*, which usually corresponds to the constant voltage sent to all actuators. With respect to the bias shape, the mirror deformation becomes bidirectional, and in practice, the squared voltage range $0 : V^2_{max}$ is converted to the control signals in the range $-1 : 1$, with 0 corresponding to the bias voltage.

Thus, for a mirror with N actuators, all possible mirror shapes form a $N-$dimensional parallelepiped in $C(\Omega)$, the functional space of continuous functions defined on Ω.

In the case of a zero gap between the actuators and a circular shape Ω, the bias corresponds to a defocus (surface of the constant positive curvature, $w(x, y) \propto x^2 + y^2$). In practice, to avoid the electrical breakthrough between the actuators, some gap, depending on the maximal voltage difference between the neighbouring actuators and on the technological limitations, is present, and the bias shape is an approximation of a defocus.

The final gap prevents the simplest approach of just filling the aperture with a lot of small actuators, as in this case, the area occupied by the dominates the active region formed by the actuators.

2.2 Method of estimating the maximal error

For a given set of mirror response functions, the maximum approximation error is estimated as follows.

First, the maximum error requirements were interpreted as the lengths of semi-axes of a hyper-ellipsoid in the Zernike polynomial space, with its centre in the point corresponding to the bias shape. Thus, any input aberration $\boldsymbol{a}$ to be corrected by the mirror is given by

$$\boldsymbol{a} = S\boldsymbol{x} + \boldsymbol{b},\ \|\boldsymbol{x}\| = 1 \tag{2}$$

where $S = D(z_1, \ldots, z_{25})$ a diagonal matrix, $\boldsymbol{x}$ is a unit-length vector, and $\boldsymbol{b}$ is the bias defocus (to be explained in the next section).

Second, neglecting the finite voltages constraint, a general mirror response is represented by a linear subspace M spanned by the mirror response functions. Then the approximation of any income aberration $\boldsymbol{a}$ is given by a projection of a point from the ellipsoid on this linear subspace, and the error is given by the projection on the space orthogonal to it:

$$\boldsymbol{\varepsilon} = (I - \Pi_M)\boldsymbol{a} = (I - \Pi_M)(S\boldsymbol{x} + \boldsymbol{b}) = L\boldsymbol{x} + (I - \Pi_M)\boldsymbol{b},\quad \|\boldsymbol{\varepsilon}\| \le \|L\boldsymbol{x}\| + \epsilon_b, \tag{3}$$

where Π_M is the projection operator on M and $L = (I - \Pi_M)S$, $\epsilon_b = \|(I - \Pi_M)\boldsymbol{b}\|$ is the error of the bias approximation with the mirror responses, and thus, all the errors also form a hyperellipsoid with its centre in $(I - \Pi_M)\boldsymbol{b}$. If the mirror can perfectly generate the bias defocus, the last term is zero, and the maximal error is given by the length of the largest singular vector of the SVD decomposition of matrix L.

2.3 Procedure for the error estimation for an arbitrary actuator layout geometry and a formal optimization problem

The following procedure has been used to estimate the maximal error of approximating an income aberration by an MMDM with a given actuator layout.

1. Define the sampling grid size and obtain a vector of "rasterized" Zernike polynomials $Z_i(x, y)$ within the mirror active aperture.
2. Use successive over-relaxation method (SOR) to solve the Poisson equation[14] on a larger grid corresponding to the whole membrane with the same sampling size for each of the actuators to find the response functions $r_n(x, y)$. Normalize the responses so their sum corresponds to the physical value of the maximum deflection $d_{\max}$ (e.g. 10μm at 300 V): $\sum_n r_n(0, 0) = d_{\max}$.
3. Add a piston term to the responses to form the approximation subspace $M = \langle 1, r_1(x, y), \ldots, r_N(x, y)\rangle$ and find the projections $\Pi_M Z_i$ and approximation errors $(I - \Pi_M)Z_i$ for all input modes and build the matrix L. Find the bias approximation ϵ_b.
4. Use thin SVD for L and estimate the maximal error using the length of the largest singular vector (plus the bias approximation error):

$$L = U\Sigma V^T,\ \Sigma = D(\sigma_1, \ldots, \sigma_{25}),\ \varepsilon \le \sigma_1 + \epsilon_b. \tag{4}$$

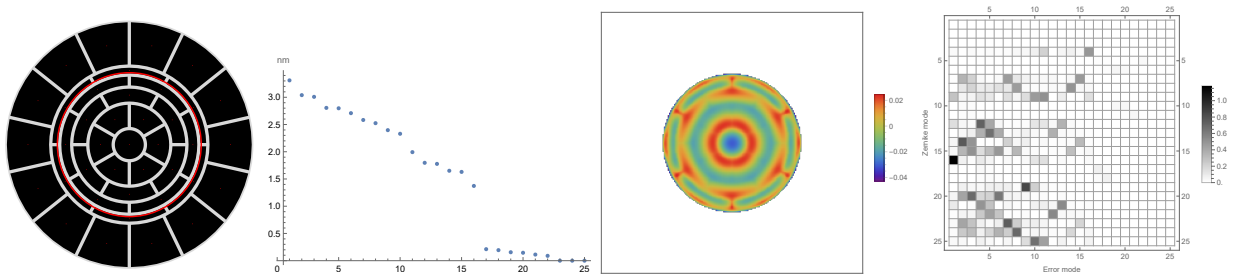

(a) (b) (c) (d)

Figure 1: Results of the approximation of the input aberration by OKO 39-ch 15mm MMDM: a) actuator geometry layout of an OKO 39-channel 15mm MMDM; red circle indicates the working aperture where the aberration is defined; b) estimated lengths of the semi-axes of the approximation error hyperellipsoid; c) the shape of the largest singular mode; d) the error dependence matrix (columns represent singular modes, rows – the Zernike polynomials)

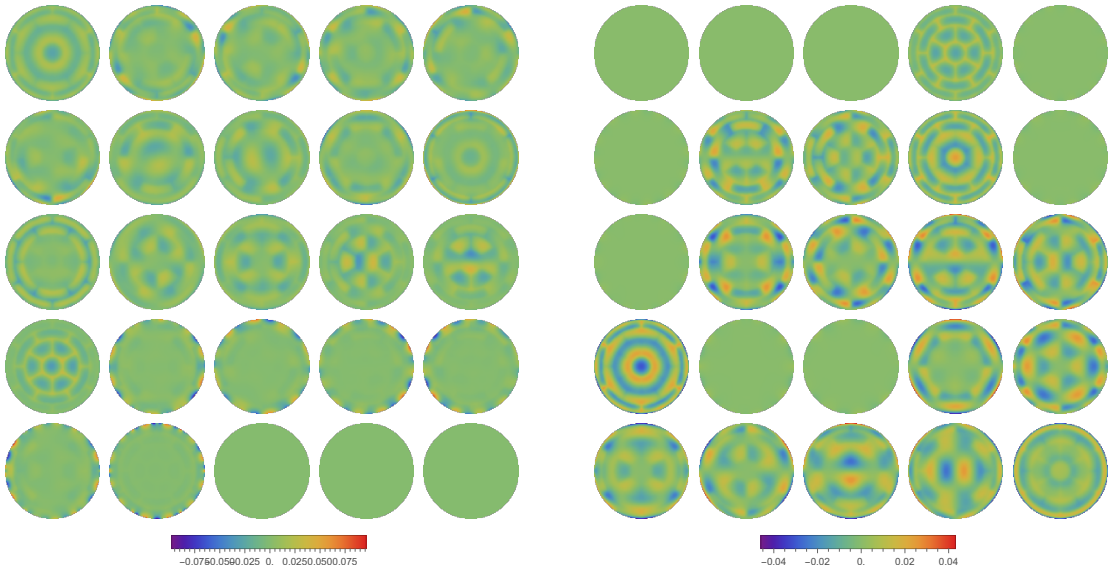

(a) Singular modes of the approximation error (b) Approximation error per Zernike mode

Figure 2: Illustration of the approximation error calculated for MMDM15-39. The plot shows the singular modes u_n of the error ellipsoid (a) and the error of approximating Z_n with requested amplitude z_n (b), for n=1, ..., 25 (left to right, top to bottom), in a common scale (in λ).

The results of such a procedure for an existing MMDM ("MMDM15-39", 15 mm membrane aperture, with 39 actuators, equal actuator areas inside the working aperture of 10 mm) are presented in Figs. 1 and 2. The first singular mode (Fig. 1c) shows the "most difficult" to be approximated by the mirror wavefront, and one can see from Fig. 1d that the main contribution to the error is made by Z_{16}, the spherical aberration. We can also investigate the approximation results by plotting the main axes of the error ellipsoid (columns of matrix U) and the error produced by each of the scaled Zernike modes (columns of L), as shown in Fig. 2 (the error is zero for piston and tip-tilt modes Z_1, Z_2, Z_3 because $z_1 = z_2 = z_3 = 0$). We can also see a significant error in the approximation of the defocus (Z_4).

Now, the task of finding an optimal actuator geometry can be formalized as follows. Let $G = \{\Omega_1, \ldots, \Omega_N\}$ be a subdivision of the mirror aperture, $\Omega = \cup_n \Omega_n$, with the boundary $\Gamma = \cup_n \partial\Omega_n$. Then optimal subdivision G minimizes the maximal error ε of Eq. (4):

$$G_{opt} = \arg\min_G \varepsilon(G) \leq \arg\min_G \ \sigma_1(G) + \epsilon_b(G). \tag{5}$$

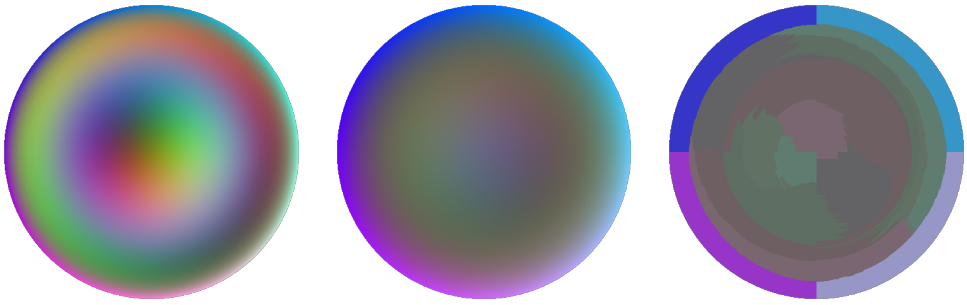

(a) (b) (c)

Figure 3: An example of an RGB image constructed by a combination of some three input Zernike polynomials of maximal amplitude (a) and their Laplacians (b). Result of colour quantization algorithm applied to combination of the Laplacians (c).

For a circular aperture Ω and a defocus bias, the rightmost term in the last equation is equivalent to the minimization of the area occupied by the gaps between the actuators, which for a fixed gap width is proportional to the total length of boundary Γ.

Optimization of the left term represents a difficult problem, and we could not find a solution in the literature. Below, we suggest some heuristic approaches that do not guarantee the optimal solution but allow us to find a geometry that better matches the requirements.

3. IMPROVEMENT OF THE ACTUATOR GEOMETRY USING ALGORITHMS FROM MACHINE-LEARNING AND IMAGE PROCESSING

Although the procedure described in the previous section can be done relatively fast (depending on the grid resolution and number of actuators, it could take up to several minutes), it is not suitable for an iterative approach for finding the optimal geometry, which minimizes the correction error. However, instead of finding the best solution, it is sufficient to find an improvement with a total error less than the requirement.

Similarly to the widely used in practice method of approximation of the wavefront gradient by the basis gradients instead of reconstruction of the wavefront by integration first and decomposition of it in the basis, we propose to simplify the task and to approximate the Laplacians of the input aberrations by those of the response functions, which are represented by piece-wise constant functions, according to Eq. (1). As we want to approximate all these Laplacian of the Zernikes jointly, the task is similar to the problem of colour quantization of a hyperspectral image composed from all Laplacians (see Fig. 3b for an example of a 3-channel image obtained by a combination of only 3 from Laplacians).

There are many algorithms developed for image segmentation, for instance, based on the minimization of the simplified Mumford-Shah functional:[10]

$$E(u,\ \Gamma) = \int_{\Omega} (u - I)^2\ dx + \mu \int_{\Gamma} d\sigma. \tag{6}$$

Here, I denotes some scalar or vector function (hyperspectral image) obtained from the Laplacians of the Zernike polynomials (in our calculations, we have used the maximal amplitude of a corresponding Zernike for each component of I, see Fig. 3).

One can easily see the similarity of Eq. (6) to the original problem of Eq. (5), but by switching to the Laplacian approximation, we can 1) avoid the costly response calculations and 2) use already developed image segmentation algorithms. Figure 3c shows an example of image segmentation algorithm ("min-variance colour quantization"[15]) applied to an example 3-channel image of Fig. 3b. One can see that the algorithm cannot perform well in the region without sharp edges in the centre, and the proposed subdivision looks random there.

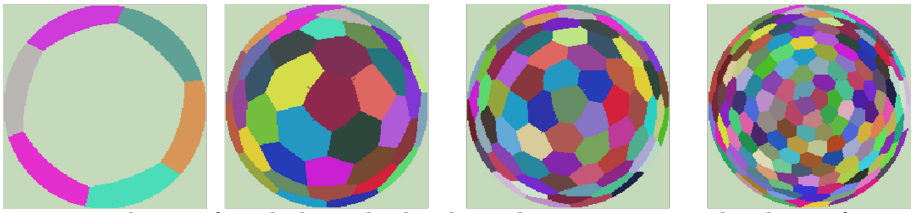

Figure 4: Some geometry layout found through the data clustering approach, shown for 7, 39, 79, and 200 actuators.

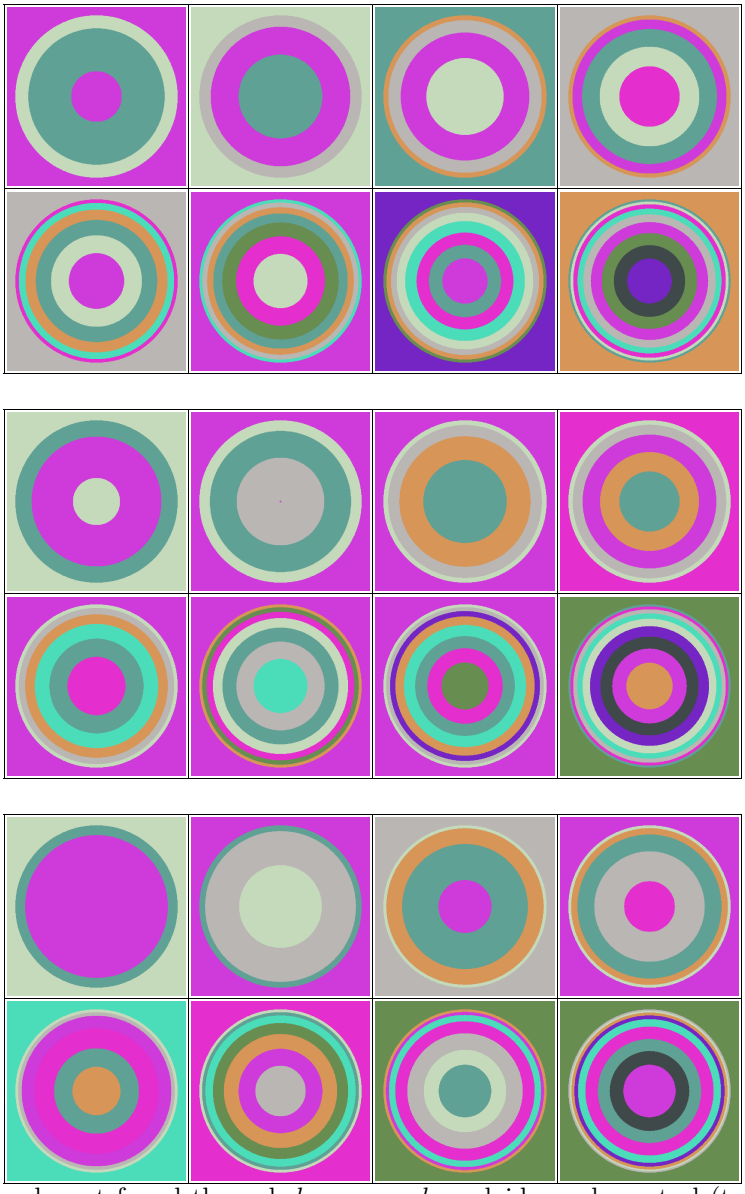

Figure 5: Some geometry layout found through $k-$means, k-medoids, and spectral (top to bottom) clustering approach, shown for 3 to 10 clusters, which can be converted to actuator rings radii.

Still, it performs well next to the edges, where the curvature changes faster, and finds some characteristic sizes in those regions.

An alternative way to find the optimal subdivision is to use machine-learning methods for data clustering.

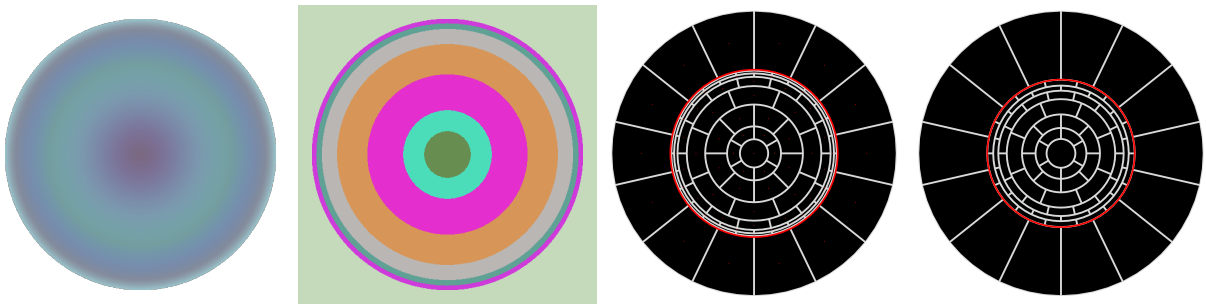

(a) (b) (c) (d)

Figure 6: Laplacians of radial parts of all input Zernikes combined in one hyperspectral image (a), segmentation obtained by k-means clustering into 7 components (b), 15-mm mirror actuator structure obtained from this subdivision (c); adjusted 30-mm MMDM actuator structure. The mirror working aperture is shown with a red outline.

Note that the clustering considers only the values of the Laplacians, and not their location, and consequently might result in intertwined actuators. We have used k-means clustering[16] for the subdivision. Interestingly, the subdivision obtained with the clustering approach features ring-like arrangements of the actuators with approximately equal arc lengths of the actuators, see Fig. 4.

Several improvements can be made to account for the best compensation of any combination of the input aberration. For our final calculations, we have used only the radial components of the input Zernikes to obtain the "characteristic radii" for the subdivision and subdivided each of the rings according to the maximal angular order of the input polynomials and approximately equal arc size of the actuators (see Fig. 6).

The obtained radial segmentation does depend on the algorithm used for the clustering, but the results obtained with the k-means and k-medoids algorithms were close to each other.

4. IMPROVED MIRROR LAYOUT

To obtain an improved mirror layout, we have selected one of the radial subdivisions for the actuator structure inside the working aperture, and subdivided each of the rings into segments of approximately equal length. For the actuators outside the working aperture, we have used the same number of actuators as in the largest ring inside the working aperture. The initial configuration is shown in Fig. 6c.

As the image segmentation algorithm does not account for the finite gap between actuators, the outer rings of actuators become too thin, and the obtained configuration was further manually readjusted, as shown in Fig. 6d. In addition, it appeared that for a 15 mm mirror, the minimal gap of 0.1 mm takes too much space and does not allow to obtain small ϵ_b. By increasing the mirror's full aperture to 30mm, we were able to achieve the target accuracy. Figure 7 compares the results of the error estimation obtained with the configurations of Fig. 6c and Fig. 6d.

It should be noted that although with the improved mirror layout, we have achieved the target requirements, the obtained configuration is not optimal in the pure mathematical sense, as it was not obtained by optimization of Eq. (5).

5. CONCLUSION

We have demonstrated a formal mathematical problem of finding an optimal MMDM actuator geometry. By using established methods from image processing and machine learning, we found an approximate solution, improved the existing MMDM actuator geometry, and reached our partners' correction accuracy requirements. However, the proposed solution might be further improved by solving the proposed minimization problem with more appropriate methods.

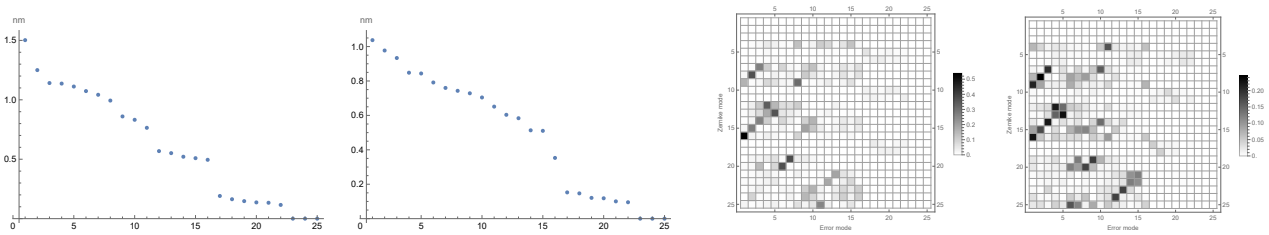

(a) Singular values

(b) Error dependence matrix

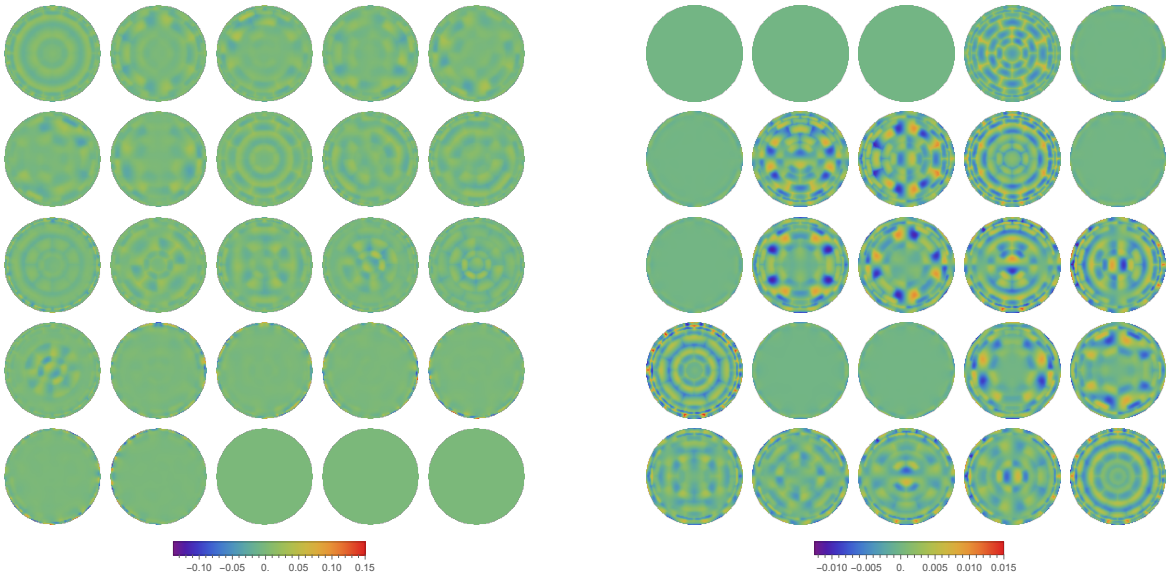

(c) Singular modes

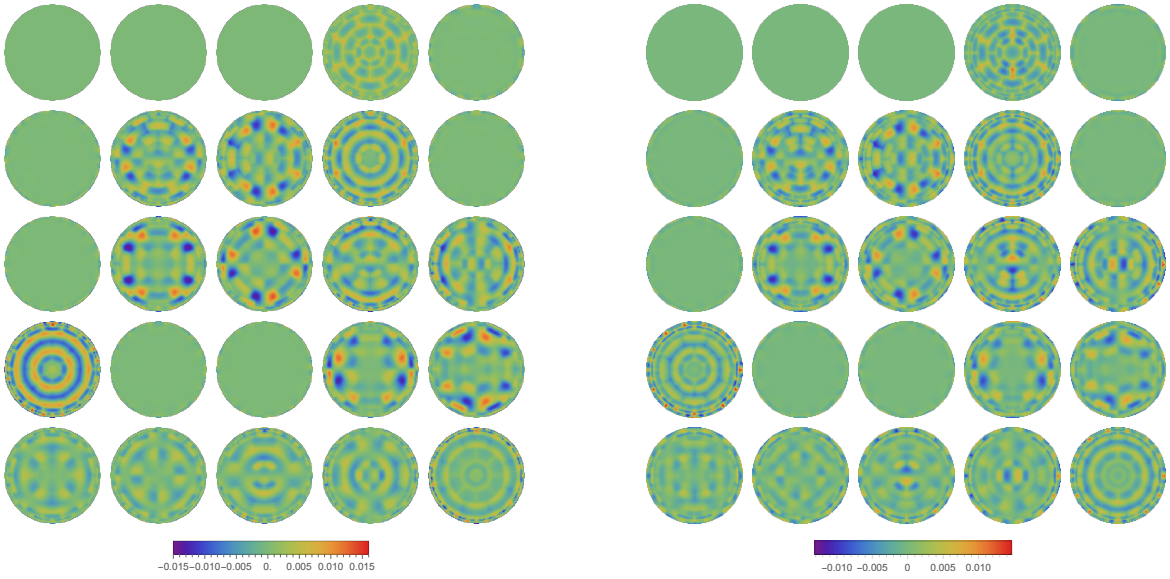

(d) Error per Zernike mode

Figure 7: Results obtained for the mirror layouts shown in Fig. 6c (left in each pair of images) and Fig. 6d (right in each pair of images)

ACKNOWLEDGMENTS

The project is supported by the Chips Joint Undertaking and its members, including the top-up funding by RVO (The Netherlands Enterprise Agency).

REFERENCES

[1] Tyson, R. K., [*Principles of adaptive optics*], CRC Press, Taylor & Francis Group, Boca Raton, fifth edition ed. (2022). Previous edition: 2016.

[2] Fernández, E. J. and Artal, P., "Membrane deformable mirror for adaptive optics: performance limits in visual optics," *Optics Express* **11**, 1056 (May 2003).

[3] Kubby, J., [*Adaptive Optics for Biological Imaging*], CRC Press, 1st edition ed. (2013).

[4] Roggemann, M. C. and Welsh, B., [*Imaging through turbulence*], CRC Press (1996).

[5] Noll, R. J., "Zernike polynomials and atmospheric turbulence*," *Journal of the Optical Society of America* **66**, 207 (Mar. 1976).

[6] Roddier, F., ed., [*Adaptive optics in astronomy*], Cambridge University Press, Cambridge [u.a.], first paperback ed ed. (2004). Literaturangaben.

[7] Loktev, M., De Lima Monteiro, D. W., and Vdovin, G., "Comparison study of the performance of piston, thin plate and membrane mirrors for correction of turbulence-induced phase distortions," *Optics Communications* **192**, 91–99 (May 2001).

[8] Vdovin, G. V., Middelhoek, S., and Sarro, P. M., "Technology and applications of micromachined silicon adaptive mirrors," *Optical Engineering* **36**, 1382 – 1390 (May 1997).

[9] Horizon Europe, "14 Angstroms Module Integration (14AMI)," online, Grant agreement ID: 101111948 (May 2023).

[10] Bar, L., Chan, T. F., Chung, G., Jung, M., Vese, L. A., Kiryati, N., and Sochen, N., "Mumford and Shah Model and Its Applications to Image Segmentation and Image Restoration," in [*Handbook of Mathematical Methods in Imaging*], 1539–1597, Springer New York, New York, NY (2015).

[11] Petitot, J., "An introduction to the Mumford-Shah segmentation model," *Journal of Physiology Paris* **97**(2-3), 335–342 (2003).

[12] Soloviev, O., "Deformable mirror characterisation using novel phase tilted interferometry (PTI) method," in [*Quantitative Phase Imaging XI*], *Proc. SPIE 13329* (2025).

[13] Vdovin, G., Soloviev, O., Samokhin, A., and Loktev, M., "Correction of low order aberrations using continuous deformable mirrors," *Optics Express* **16**, 2859 (mar 2008).

[14] Press, W. H., Teukolsky, S. A., Vetterling, W. T., and Flannery, B. P., [*Numerical Recipes 3rd Edition: The Art of Scientific Computing*], Cambridge University Press, 3 ed. (2007).

[15] Wu, X., "Color quantization by dynamic programming and principal analysis," *ACM Transactions on Graphics* **11**, 348–372 (Oct. 1992).

[16] Theodoridis, S., "Bayesian Learning: Inference and the EM Algorithm," in [*Machine Learning*], 595–646, Elsevier (2020).